The Planetary Science Journal, 7:158 (8pp), 2026 June https://doi.org/10.3847/PSJ/ae6faa

Environmental Effects on Space-weathered Lizardite Grains

Nicole M. Ozdowski[1], Ian J. Marrs[1], Max A. Hood[1,2], Mark R. Salvatore[1], Cristina A. Thomas[1], and Mark J. Loeffler[1,3]
[1] Department of Astronomy and Planetary Science, Northern Arizona University, Box 6010, Flagstaff, AZ 86011, USA
[2] Department of Astronomy, University of Maryland, 4296 Stadium Dr., Physical Sciences Complex (Building 415), Room 1113, College Park, MD 20742, USA
[3] Center for Materials Interfaces in Research and Applications, Northern Arizona University, Flagstaff, AZ 86011, USA
Received 2025 October 10; revised 2026 May 5; accepted 2026 May 13; published 2026 June 24

Abstract

Sample preparation is a crucial step in the analysis of returned material from asteroid surfaces, such as Bennu and Ryugu. Here, we study the effect of soaking olivine and lizardite in H_2O after they have been irradiated with 4 keV He^+ ions. We find that soaking depletes the irradiated surface of Mg and that the depletion depends on both the ion fluence and the soak time. Specifically, we find that only 5 minutes of soaking can result in as much as 45% Mg depletion, while longer soak times can deplete the Mg further. Our results imply that returned samples from asteroids containing olivine or lizardite will be susceptible to Mg loss if they are soaked in H_2O prior to analysis. Finally, we note that this depletion may also occur for other cations besides Mg, suggesting that careful attention should be paid to the handling of any extraterrestrial sample that requires some form of sample preparation prior to analysis.

Unified Astronomy Thesaurus concepts: Space weather (2037); Asteroid surfaces (2209); Experimental data (2371); Surface processes (2116); Asteroids (72); Photoelectron spectroscopy (2097)

1. Introduction

The surfaces of airless bodies in our solar system undergo geochemical changes through a variety of processes collectively referred to as space weathering (B. Hapke 2001; C. R. Chapman 2004; C. M. Pieters & S. K. Noble 2016). For bodies such as the Moon, main belt asteroids, and near Earth asteroids (NEAs), the primary surface-altering effects are understood to be solar wind irradiation and micrometeorite impacts (B. Hapke 2001; C. R. Chapman 2004; M. J. Loeffler et al. 2009).

Much of our understanding of space weathering and its effect on small airless bodies comes from the study of lunar samples (B. Hapke 2001). Comparison of returned lunar rock and fine-grained samples reveals that space weathering effects lower the albedo, redden the slope, and diminish the absorption-band depth of the infrared spectra of the fine-grained samples (J. B. Adams & R. L. Jones 1970; B. Hapke 1970). Redeposited material can also form compositionally distinct coatings from bulk lunar grains, often containing microphase and nanophase iron inclusions (L. P. Keller & D. S. McKay 1993, 1997; S. J. Wentworth et al. 1999).

Laboratory simulations of space weathering show that solar wind irradiation can induce darkening and reddening in samples containing iron (B. Hapke 2001; R. Brunetto & G. Strazzulla 2005; M. J. Loeffler et al. 2009), as well as the chemical reduction of iron to its metallic state (C. A. Dukes et al. 1999). Laser irradiation experiments have been used to simulate the effects of micrometeorite impacts (S. Sasaki et al. 2003; R. Brunetto et al. 2006; M. J. Loeffler et al. 2008; M. Matsuoka et al. 2020; B. S. Prince et al. 2020; M. S. Thompson et al. 2020), as well as the role of vapor redeposition (M. J. Loeffler et al. 2008). Both types of studies show that the altered material and vapor deposits are redder, darker, and have attenuated absorption bands compared to their pristine counterparts. Follow-up microscope analysis also reveals the presence of micro- to nanophase metallic iron particles (S. Sasaki et al. 2003; M. J. Loeffler et al. 2008, 2016).

While formation of chemically reduced iron appears to be the dominant chemical change induced by space weathering, there have also been seemingly conflicting reports about whether space weathering can also change the Mg abundance in terrestrial analogs (J. P. Bradley 1994; C. A. Dukes et al. 1999; K. Demyk et al. 2001; C. Jäger et al. 2003; N. Bott et al. 2024), as well as in processed interplanetary dust (J. P. Bradley 1994). Specifically, some reports showed there to be little change in the Mg abundance (C. A. Dukes et al. 1999; C. Jäger et al. 2003), while others (J. P. Bradley 1994; K. Demyk et al. 2001) reported significant (up to 40%) or even complete Mg depletion in analyzed samples (J. P. Bradley 1994; N. Bott et al. 2024).

E. D. Cantando et al. (2008) hypothesized that the reported differences in Mg abundances in olivine samples could be a consequence of environmental effects, as some studies had the ability to perform the analysis without removing the altered samples from the vacuum environment, while other studies removed the sample from vacuum prior to analysis. Their hypothesis arose from experiments showing that soaking olivine samples irradiated with 4 keV Ar^+ in H_2O caused up to 60% Mg depletion. However, we point out that while rinsing irradiated olivine does promote Mg depletion, it does not explain the differences in literature, as none of the above studies explicitly say that they rinsed their samples prior to analysis.

Regardless, understanding how space-weathered minerals respond to sample preparation methods, such as exposure to H_2O, is even more important in the current context, as there are multiple missions such as OSIRIS-REx and Hayabusa2 that aim to bring, or have already brought, samples back from small airless bodies that have presumably been exposed to

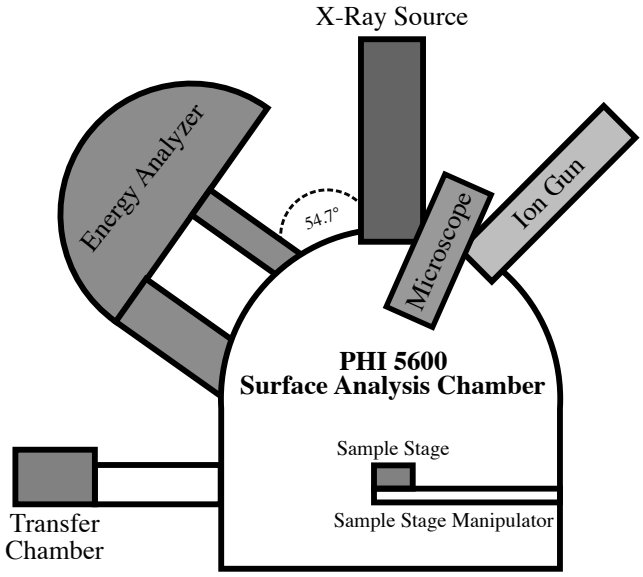

Figure 1. Schematic of our Perkin-Elmer PHI 5600 surface analysis system. The angle between the ion gun and sample surface is 45°.

some form of space weathering (T. Yada et al. 2022; D. S. Lauretta et al. 2024). In this study, we used X-ray photoelectron spectroscopy (XPS) to monitor, in situ, the surface composition of terrestrial samples of olivine and serpentine during irradiation with 4 keV He^+ ions to simulate solar wind irradiation. Following irradiation, we removed the sample from vacuum and studied the effect of exposing it to H_2O. We focused on phyllosilicates here, as they are believed to be widespread on the surfaces of carbonaceous asteroids (F. DeMeo et al. 2015; D. Takir et al. 2015; A. S. Rivkin et al. 2019) and have been detected in returned samples from asteroids Bennu and Ryugu (D. S. Lauretta et al. 2024; T. Noguchi et al. 2024).

2. Experimental Methods

2.1. Sample Preparation

We performed our experiments on Twin Sisters olivine and serpentine. We obtained the olivine samples from Millbank Materials and the serpentine samples from Hausen Rock Treasures, originally gathered in Norway. Typically, we used 3 mm grains for our experiments. Prior to the experiments, we cleaned all grains in an ultrasonic bath, using a triple wash cycle of acetone, isopropanol, and high-performance liquid chromatography (HPLC) H_2O. After cleaning the samples and allowing them to dry under ambient conditions, we mounted a sample grain onto the sample stage using either carbon tape or copper metal clips. Both mounting approaches produced consistent results in our H_2O soaking experiments presented here. However, we only used the metal clips when we soaked the irradiated sample in acetone and isopropyl alcohol, because we found that the sample often shifted on (and sometimes dislodged from) the carbon tape when we soaked it in these solvents. After mounting the grain, we then inserted it into our PHI 5600 surface analysis system (Figure 1), which operates at a base pressure of approximately 10^{-9}–10^{-10} Torr.

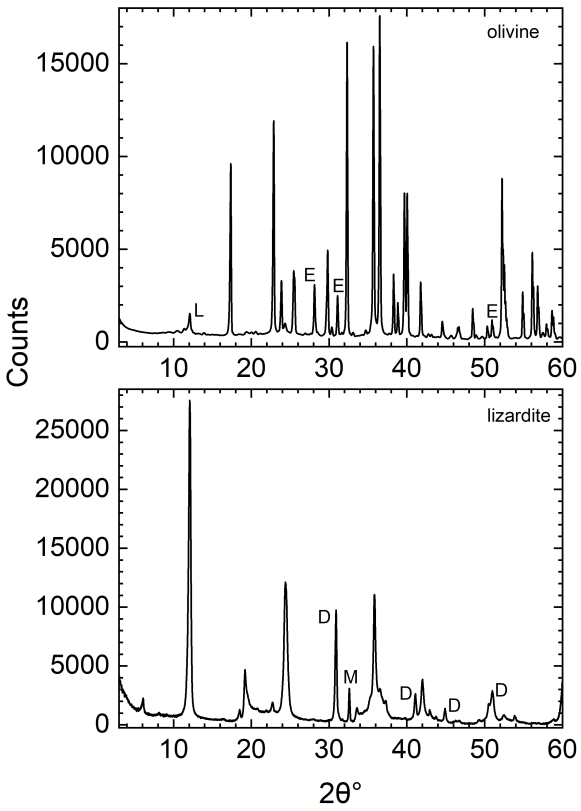

Figure 2. X-ray diffraction pattern for our olivine (top) and lizardite (bottom) samples. Lizardite and enstatite peaks in the olivine pattern have been marked with "L" and "E." Dolomite and magnesite peaks in the lizardite pattern have been marked with "D" and "M."

2.2. X-Ray Diffraction of Bulk Samples

To perform X-ray diffraction (Rigaku Miniflex4) on our samples (Figure 2), we crushed the grains down into a powder (Twin Sisters olivine (45–125 μm) and serpentine (<45 μm)). The olivine sample's pattern is consistent with forsterite and minor amounts of enstatite and lizardite. Such impurities are expected, since the Twin Sisters deposits are enstatite-bearing dunites (0%–20% enstatite) with widespread serpentinization observed (D. M. Ragan 1963). The serpentine sample's pattern is consistent with lizardite and minor amounts of magnesite and dolomite. These impurities are also expected, since the serpentinization process can easily liberate Ca^{2+} and Mg^{2+} from the host rock, which can combine with the dissolved CO_2 or CO to form carbonate minerals (M. O. Schrenk et al. 2013; R. Lafay et al. 2014).

2.3. X-Ray Photoelectron Spectroscopy, Ion Irradiation, and Postirradiation Soaking

We used XPS to monitor the surface composition of our sample grains before, during, and after irradiation. XPS is sensitive to the top several nanometers of a sample's surface and has been used regularly to analyze changes in minerals induced by space weathering processes (C. A. Dukes et al. 1999; C. Davoisne et al. 2008; L. C. Chaves et al. 2023). In this study, we took survey and high-resolution (HR) XPS spectra of our samples using Mg Kα X-rays (1253.6 eV). For survey spectra, we took 1 eV steps with a dwell time of 50 ms $step^{-1}$ and a pass energy of 117.4 eV (energy resolution <1.8 eV), and then averaged between four and eight scans,

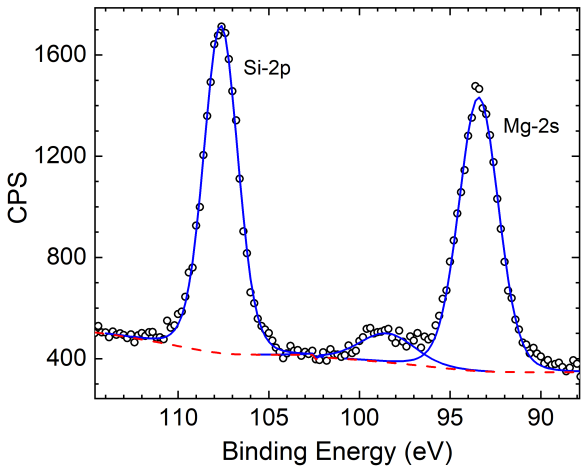

Figure 3. Representative Shirley background subtraction and peak fitting done via CASA XPS on lizardite. Open circles represent recorded data, and the red dotted line represents the Shirley background. After the background subtraction, we used Gaussian fits to calculate the band areas for the Si 2*p* and Mg 2*s* features (blue solid lines). While we fit the Si 2*p* area with one Gaussian fit, the Mg 2*s* area always included a smaller shake-up peak at higher binding energy.

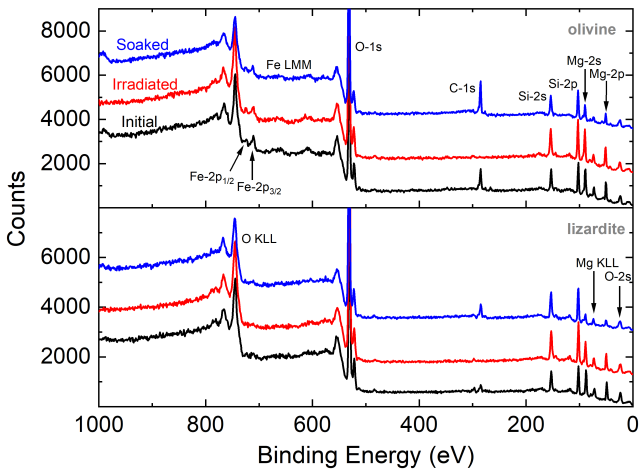

Figure 4. XPS survey spectra of olivine (top) and lizardite (bottom) before irradiation (black line), after irradiation with 8.29×10^{16} He^{+} cm^{-2} (red line), and then after soaking it in HPLC H_2O for 5 minutes (blue line). The three spectra have been vertically offset for clarity.

depending on the quality of the data. We acquired the HR data in 0.2 eV steps with a dwell time of 50 ms $step^{-1}$ and a pass energy of 46.95 eV (~0.7 eV energy resolution), and then averaged over 12 scans for the C 1*s* feature, 6 scans for the O 1*s* feature, 30 scans for the Mg 2*s* and Si 2*p* features, and 36 scans for the Fe 2*p* feature (in olivine). We chose these peaks because they are representative of the main components consistently observed in the survey spectra of our samples. While we did identify a minor amount of dolomite, $MgCa(CO_3)_2$, in our lizardite sample via X-ray diffraction, we only occasionally detected a weak band at ~347 eV indicative of calcium. As XPS is ~6 times more sensitive to this Ca 2*p* transition than it is to the Mg 2*s* and Si 2*p* transitions reported here (J. F. Moulder et al. 1992), it is not surprising that samples containing this minor surface impurity showed the same trends as those that did not.

We calibrated the binding energy scale by horizontally shifting our data so that our adventitious carbon (C 1*s*) feature appeared at 284.8 eV (C. J. Powell et al. 1979). We analyzed all XPS spectra using a Shirley background subtraction (D. A. Shirley 1972) via CASA XPS (N. Fairley et al. 2021) and used the resulting band areas to calculate atomic concentrations for each element from the expression $C_x = (I_x/S_x)/(\Sigma I_i/S_i)$, where C_x is the atomic concentration of a particular element x, I is the band area of a particular element, and S is the atomic sensitivity factor for our system (J. F. Moulder et al. 1992). We always included the Mg 2*s* shake-up peak (appearing at a higher binding energy) in our band area analysis, as this peak is formed by photoelectrons that lost energy while escaping the Mg 2*s* orbital. Figure 3 provides an example of this analysis process using CASA XPS on a lizardite sample. After irradiation had removed the C 1*s* peak, we shifted XPS spectra so that the O 1*s* peak in the irradiated sample appeared at the same binding energy as the fresh sample.

To simulate the solar wind environment, we used a differentially pumped ion gun (Perkin-Elmer 04-303A) to irradiate our samples with 4 keV He^{+} ions at a flux of 8.6×10^{13} He^{+} cm^{-2} s^{-1}. We produced He^{+} ions by leaking He gas (99.999% purity) into the ion gun and measured the ion flux by placing a Faraday cup in the sample position. To calculate the total fluence (ions cm^{-2}), we multiplied the ion flux, which varied less than 10%, by the irradiation time. We also rastered the ion beam over a region of at least 3 × 3 mm to ensure the sample was uniformly irradiated over an area larger than the analysis area (1 mm). We estimate that these ions penetrate up to 50 nm (in olivine) and 60 nm (in lizardite) below the surface (J. F. Ziegler et al. 2010), which is more than an order of magnitude deeper than the estimated analysis depth of XPS for our elements of interest (M. P. Seah & W. A. Dench 1979). After irradiation and XPS analysis, we removed the sample from vacuum and soaked it in either HPLC H_2O, high-purity (99.9%) acetone, or high-purity (99.9%) isopropyl alcohol for a prespecified time interval. We then reintroduced it into vacuum for follow-up XPS analysis. In all of our experiments, we imaged our sample with an in situ microscope to ensure that we could put it back into nearly the same position (within ~70 μm) after reintroducing our sample into the vacuum system.

2.4. Initial Checks and Control Experiments

Prior to our irradiation experiments, we studied how much the Mg concentration varied from sample to sample and whether soaking unirradiated samples caused changes in the Mg concentration. We found as much as 20% variation in the initial Mg concentration in olivine, and that slicing the samples reduced the variation slightly to about 15%. Our lizardite samples were too small to easily slice, so we took advantage of the small analysis area of our XPS instrument and simply moved our sample until we found a composition that was within ~15% to other experiments. Finally, we found that soaking the olivine and lizardite prior to irradiation caused minimal change in the Mg concentration, as it remained constant within ~10%.

3. Results

In Figures A1 and A2, we show five different starting XPS survey and HR spectra representative of the olivine and lizardite samples used in this study, while Figures 4 and 5

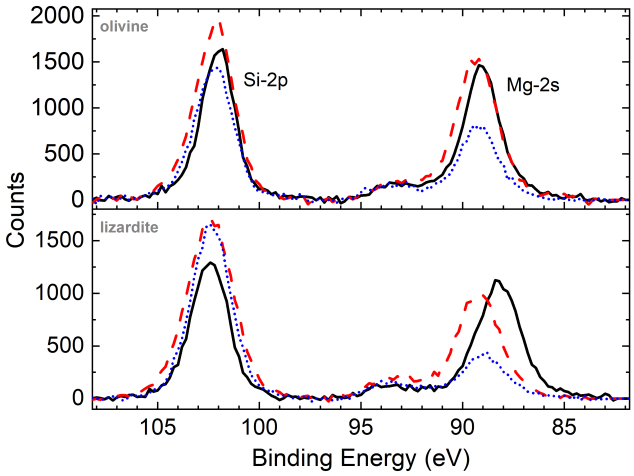

Figure 5. XPS continuum-removed HR spectra of olivine (top) and lizardite (bottom) before irradiation (solid black line), after irradiation with 8.29×10^{16} He^{+} cm^{-2} (dashed red line), and then after soaking it in HPLC H_2O for 5 minutes (dotted blue line).

show XPS survey and HR spectra for representative olivine and lizardite grains before and after irradiation with He^{+} ions, as well as after soaking the irradiated samples in HPLC H_2O for 5 minutes. As expected, the main components in each sample are O, Si, Mg, and Fe (in olivine). Both samples also have a carbon feature, which we attribute to adventitious carbon (C. J. Powell et al. 1979; C. A. Dukes et al. 1999; M. J. Loeffler et al. 2009). These spectra show that irradiation removes most of the carbon layer in our samples, as well as chemically reducing the iron in the olivine. Furthermore, we also find that the combination of ion irradiation and soaking causes the iron in the olivine to reoxidize, in addition to causing a significant decrease in the Mg photoelectron peaks in both samples.

To quantify the spectral changes noted above, we measured the band area of the O 1*s*, Si 2*p*, Mg 2*s*, Fe 2*p* (for olivine), and C 1*s* peaks in the olivine and lizardite samples and converted those values to atomic concentration (Figure 6). For olivine, we removed the adventitious carbon after 4×10^{16} He^{+} cm^{-2}. As expected, the removal of carbon corresponds to an increase in the other components intrinsic to the olivine. After carbon is removed, the concentration of Mg remains constant, while the concentration of Si slowly increases by ~6% and the concentration of O peaks and subsequently decreases by ~3%. The small change in the concentration of these species may be due to preferential removal of the oxygen bound to silicon. For lizardite, we removed the adventitious carbon down to an equilibrium level by 2×10^{16} He^{+} cm^{-2}. As with the olivine, the removal of carbon corresponds to an increase in the intrinsic components in lizardite. However, while the increases in the concentration of Si and O are qualitatively similar to olivine, we found that Si concentration increases by about 17% after the carbon has reached equilibrium. We suspect that this additional increase is a combination of the loss of oxide (as observed in olivine) and the ~10% decrease of Mg at the surface. The short-lived decrease in Mg suggests that our lizardite grains have a very thin layer of Mg-enriched material on the surface. We suspect that this could be magnesite ($MgCO_3$) rather than dolomite, as the observed Mg trend is reproducible, even when we do not see calcium in our XPS spectra. Regardless, the relatively large increase in Si

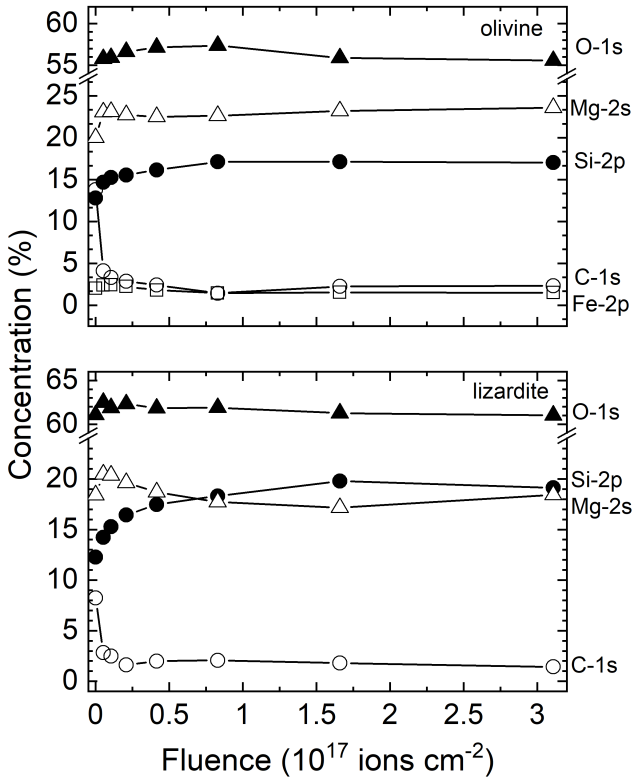

Figure 6. Concentration of O (filled triangles), Mg (open triangles), Si (filled circles), Fe (open squares), and C (open circles) in olivine (top) and lizardite (bottom) samples during irradiation with 4 keV He^{+}.

during irradiation of lizardite led us to focus our analysis in terms of concentrations, rather than atomic ratios, which have been employed previously.

With the XPS HR data, we quantified the Mg concentration in olivine and lizardite as a function of ion fluence and subsequent soaking, where we soaked the irradiated sample in HPLC H_2O for 5 minutes (Figure 7). We chose 5 minutes of soaking because this is a typical time that could be used to wash a sample in the laboratory. For both samples, the Mg concentration always begins within and stays within the figure's shaded region during irradiation. However, soaking the irradiated samples causes a significant decrease in the Mg concentration, and we assume that this decrease extends through the entire depth penetrated by our ions, as was noted by E. D. Cantando et al. (2008).

To quantify this effect further, we compare the average starting concentration before irradiation for a set of specific experiments to their average concentration after irradiation and soaking. For olivine, the decrease becomes noticeable after a fluence of 2.6×10^{15} ions, where soaking causes a 15% depletion (20%–17%) in the Mg concentration. The effect of soaking saturates after 2.6×10^{16} ions, where it causes the concentration to decrease by 46% (21%–14%). Lizardite behaves similarly to olivine, and at higher fluences the Mg concentration has dropped by 44% (18%–10%). Interestingly, the overall shape of the depletion curve for each sample is similar, and the fluence needed to deplete Mg in each sample halfway to their equilibrium level is nearly the same (4.2×10^{15} ions cm^{-2} for olivine and 4.4×10^{15} ions cm^{-2} for lizardite), suggesting that the rate of dissolution in H_2O is nearly the same for each mineral.

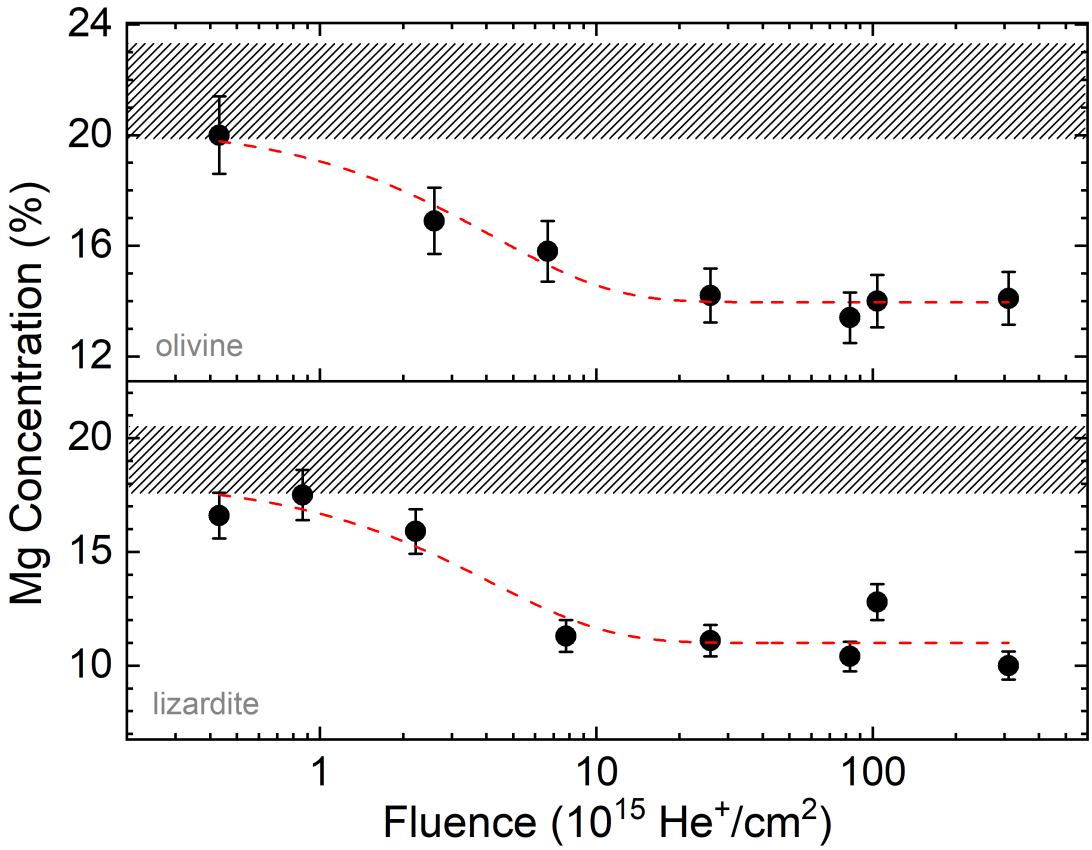

Figure 7. Mg concentration in olivine (top) and lizardite (bottom) samples as a function of irradiation fluence and subsequent soaking. We soaked all samples in HPLC H_2O for 5 minutes. The black circles represent the Mg concentration after soaking, while the shaded bar represents the range of measured Mg concentrations before and after irradiation. We have included a fitted curve (red dotted line) to guide the eye. Each black circle reflects the average final Mg concentration from all repeated experiments. Error bars reflect the largest standard error calculated in repeated experiments.

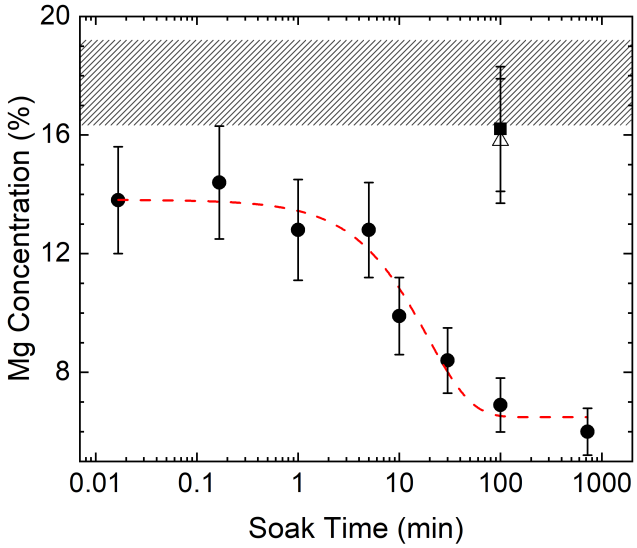

Figure 8. Mg concentration in lizardite as a function of soak time in HPLC H_2O (solid circles), high-purity acetone (open triangle), and high-purity isopropyl alcohol (closed square). Prior to soaking, we irradiated each sample with 1.0×10^{17} He^+ cm^{-2}. Each data point reflects the average final Mg concentration from all repeated experiments. Error bars reflect the standard error calculated from repeated experiments, while the shaded gray bar represents the range of measured Mg concentrations before and after irradiation. For the soaking experiments in HPLC H_2O, we have included a fitted curve (red dotted line) to guide the eye.

We also used the XPS HR data to quantify the Mg concentration as a function of soak time after irradiating lizardite with 1×10^{17} He^+ cm^{-2} (Figure 8). There is notable depletion even when the sample is dipped in H_2O (22% decrease, from 18% to 14%), which remains constant at soak times of less than a minute. However, as the soak time increases further, the Mg concentration continues to decrease. Soak times of >100 minutes caused a decrease of up to 68% (19%–6%). It is possible that longer soak times could cause more depletion, but we considered those soak times to be unlikely in regard to sample preparation.

Given the observed decrease in Mg described above, we also performed several experiments where we soaked our irradiated lizardite in high-purity acetone and isopropyl alcohol (Figure 8), two solvents widely used in sample preparation. Interestingly, even after a relatively high irradiation fluence (1.0×10^{17} He^+ cm^{-2}) and a long soak time (100 minutes), we find that (within error) soaking irradiated lizardite in these solvents causes no change in the Mg abundance.

4. Discussion

Our results show that after the removal of adventitious carbon, irradiating olivine and lizardite produces minimal changes in Mg surface concentration, consistent with previous studies (C. A. Dukes et al. 1999; C. Jäger et al. 2003; M. J. Loeffler et al. 2009; Y. Nakauchi et al. 2021). However, soaking irradiated olivine and lizardite samples in HPLC H_2O causes a significant

decrease in the Mg surface concentration, and we assume that this decrease extends the entire depth penetrated by our ions, as was noted by E. D. Cantando et al. (2008). The extent of this depletion depends on both the irradiation fluence and the soak time. Below we compare our results to previous studies, discuss possible mechanisms driving this depletion, and place our results in context with airless bodies of interest.

4.1. Comparison to Previous Experiments

E. D. Cantando et al. (2008) showed that soaking ion-irradiated olivine in HPLC H_2O caused the Mg:Si ratio in the sample to decrease by up to 60%. This is similar to our experiments, as the maximum decrease in atomic concentration (∼45%) we observed corresponds to a decrease in the Mg:Si ratio of ∼38%. The slightly lower depletion in our experiments may be due to He depositing less energy near the surface compared to Ar ions (J. F. Ziegler et al. 2010) In addition, we also find that in both studies the olivine depletes halfway to equilibrium at a similar fluence (∼4×10^{15} ions cm^{-2}).

Our soaking results for lizardite are also comparable with what has been found for olivine (E. D. Cantando et al. 2008), although it appears that the decrease in Mg in olivine may reach equilibrium after shorter soaking times. Specifically, E. D. Cantando et al. (2008) observed that the Mg:Si ratio rapidly decreased after ∼1 minute of soaking and reached equilibrium after ∼2 minutes of soaking. We find that the rapid decrease occurs after ∼5 minutes of soaking and takes ∼100 minutes of soaking to reach equilibrium.

Regardless of the minor differences described above, these two studies clearly show that soaking ion-irradiated silicates (olivines and serpentines) in HPLC H_2O can cause a significant decrease in Mg at the respective mineral's surface.

4.2. Depletion Mechanism

Many studies have shown that olivine will dissolve in acidic solutions without ion irradiation (A. Blum & A. Lasaga 1988; R. A. Wogelius & J. V. Walther 1991; O. S. Pokrovsky & J. Schott 2000a, 2000b). A. Blum & A. Lasaga (1988) proposed that this process begins with two H^+ from the acid solution replacing Mg^{2+} in the mineral. Follow-up studies support this hypothesis and show that eventually the mineral will begin to dissolve, as evidenced by the appearance of silica in the solution (A. Blum & A. Lasaga 1988; O. S. Pokrovsky & J. Schott 2000b). Some of the dissolved silica may recondense to reform a silica-rich layer that slows the overall reaction process (O. S. Pokrovsky & J. Schott 2000a; D. Daval et al. 2011).

Acidic solutions are also known to be an effective way to leach Mg from serpentine minerals (K. Kosuge et al. 1995; G. Alexander et al. 2007; S. Teir et al. 2007; K. Yoo et al. 2009). In fact, at room temperature, the most effective acids could remove about 25% of the Mg within about an hour, while at higher temperatures (70°C) nearly all the Mg could be leached within the same amount of time (S. Teir et al. 2007). Interestingly, over the timescales studied, S. Teir et al. (2007) found minimal amounts of silica in solution, in contrast to the olivine studies. Model fits to kinetic data suggested that the reaction starts at the surface and passes to the interior, slowing somewhat as the Mg-free silica layer builds up and the surface area of the reactive sites decreases (S. Teir et al. 2007). Whether this mechanism is different from what is happening in the olivine is unclear, as in both cases, one is left with an amorphous silica layer depleted in Mg.

Placing olivine in neutral solutions can also cause some Mg loss over longer timescales (O. S. Pokrovsky & J. Schott 2000b), although the rates are orders of magnitude lower than for stronger acids. Interestingly, E. D. Cantando et al. (2008) estimated that ion irradiation of olivine increased the reaction rates by 4 orders of magnitude compared to that estimated for neutral solutions, which is consistent with our results for both lizardite and olivine. They suggested that radiation damage caused by the ions breaking superficial bonds likely allows H^+ to penetrate more easily into the solid and exchange with the Mg^{2+}. That radiation damage makes it easier to remove Mg from the mineral is also consistent with what was observed by R. A. Kleiv & M. Thornhill (2006), who showed that mechanical activation (milling olivine samples) caused the rate of the initial phase of olivine dissolution (Mg removal) to increase disproportionally to measured changes in the surface area.

Finally, we suspect that the resulting surface chemistry of our samples is likely similar to the acid soaking studies described above. Although, like E. D. Cantando et al. (2008), we found no broadening in the O 1*s* peak in our depleted samples, which is different from O. S. Pokrovsky & J. Schott (2000a), who saw peak broadening and suggested it was due to H^+ penetration and/or the polymerization of silica units.

4.3. Astronomical Implications

Analysis of our laboratory data shows that irradiated samples of olivine and lizardite can show significant depletion in superficial Mg after soaking in HPLC H_2O on relatively short timescales. Specifically, we find that both samples reach equilibrium depletion of ∼45% after a fluence of 2.2×10^{16} He^+ cm^{-2} and soaking for 5 minutes. Long soak times may produce even more Mg depletion, as we observed in lizardite.

We can scale our measured fluence to an exposure time in space using the values for the mean number density (n cm^{-3}) and mean velocity (468 km s^{-1}) of protons given by J. T. Gosling (2014) at 1 au. With these values, we obtain a proton flux of 4.1×10^8 protons cm^{-2} s^{-1}. Multiplying this value by the relative abundance of He ions in the solar wind (4.7%), we estimate an incident flux of helium of 1.9×10^7 He cm^{-2} s^{-1}. For an airless body, we scale the flux down by a factor of 4, as it will be averaged over the surface area (M. J. Loeffler et al. 2009). Considering the additional slight attenuation of the flux for NEAs, such as Bennu and Ryugu, located near 1.1 au (D. S. Lauretta et al. 2015; M. Kanamaru et al. 2021), we estimate a flux of 3.9×10^6 He^+ cm^{-2} s^{-1}. A fluence of 2.2×10^{16} He^+ cm^{-2} will be reached in only about 180 yr.

Given the short exposure time for this effect to occur, we speculate that exposing any extraterrestrial olivine or serpentine mineral to H_2O will likely produce Mg loss. In fact, given that other investigations have shown other minerals can be leached of cations, besides Mg, when they are placed in acid solutions (J. F. Banfield et al. 1995; E. S. Chardon et al. 2006; S. Teir et al. 2007), we speculate that any extraterrestrial sample coming in contact with liquid H_2O may experience changes in the surface chemistry not representative of the space environment.

5. Conclusion

We studied the effects of soaking olivine and lizardite in H_2O after they have been irradiated with 4 keV He^+ ions. For both samples we find that the depletion depends both on the irradiation fluence and the soak time. After soaking our irradiated samples for 5 minutes, a number that would be

reasonable for sample preparation, we find that the Mg is depleted by as much as 45%. Longer soak times (>100 minutes) produced significantly more depletion in our lizardite samples, suggesting that given enough time, Mg may be completely removed from the region that has been damaged by ion irradiation. Interestingly, we also find that the rate of depletion is nearly the same for these two minerals, suggesting that the removal mechanism is likely the same.

Scaling our results to solar wind exposure near 1 au, we find that only 180 yr of solar wind irradiation are needed to produce our maximal observed Mg depletion (after soaking in H_2O for 5 minutes). Thus, we speculate that exposing any returned samples containing these minerals to H_2O will likely produce Mg loss. Furthermore, based on other studies showing that other minerals can also be leached of cations besides Mg, we speculate that any extraterrestrial mineral may be susceptible to surface chemistry changes not representative of the space environment if they are exposed to H_2O prior to analysis. Thus, these results should have significant implications for sample return missions, primarily those that may require some form of sample preparation prior to analysis.

Acknowledgments

This research was supported by Project ESPRESSO, a SSERVI program at SwRI under the cooperative agreement No. #80ARC0M0008 and NASA Solar System Workings Award #80NSSC22K1375. Data can be found in Northern Arizona University's long-term repository (https://openknowledge.nau.edu/id/eprint/6341).

Appendix

To show the extent of the compositional variation in our samples used in this study, we plot XPS survey and HR spectra for five representative olivine and lizardite samples prior to irradiation in Figures A1 and A2.

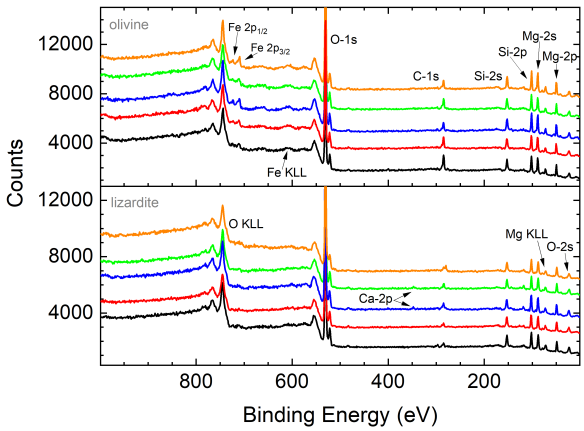

Figure A1. XPS survey spectra of different olivine (top) and lizardite (bottom) samples prior to irradiation. The Mg concentration in each sample fits within the shaded regions shown in Figures 7 and 8.

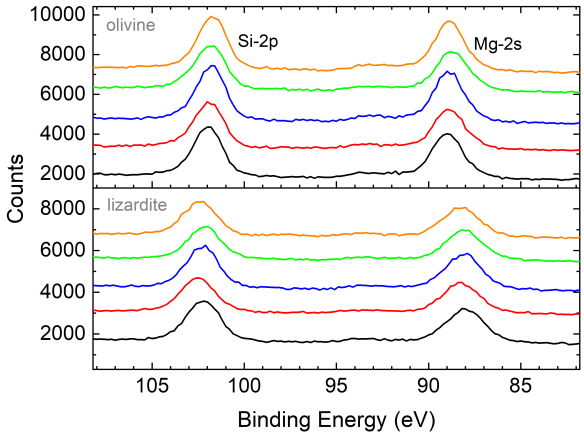

Figure A2. XPS HR spectra of the olivine (top) and lizardite (bottom) samples prior to irradiation shown in Figure A1.

ORCID iDs

Nicole M. Ozdowski https://orcid.org/0009-0008-0552-4205
Ian J. Marrs https://orcid.org/0000-0002-7154-5011
Max A. Hood https://orcid.org/0009-0009-6565-5204
Mark R. Salvatore https://orcid.org/0000-0002-1551-8342
Cristina A. Thomas https://orcid.org/0000-0003-3091-5757
Mark J. Loeffler https://orcid.org/0000-0002-1551-3197

References

Adams, J. B., & Jones, R. L. 1970, Spectral Reflectivity of Lunar Samples, Sci, 167, 737
Alexander, G., Maroto-Valer, M. M., & Gafarova-Aksoy, P. 2007, Evaluation of Reaction Variables in the Dissolution of Serpentine for Mineral Carbonation, Fuel, 86, 273
Banfield, J. F., Ferruzzi, G. G., Casey, W. H., & Westrich, H. R. 1995, HRTEM Study Comparing Naturally and Experimentally Weathered Pyroxenoids, GeCoA, 59, 19
Blum, A., & Lasaga, A. 1988, Role of Surface Speciation in the Low-temperature Dissolution of Minerals, Natur, 331, 431
Bott, N., Thompson, M. S., Loeffler, M. J., Vander Kaaden, K. E., & McCubbin, F. M. 2024, Understanding the Effects of Micrometeoroid Bombardment on Graphite-rich Mercury Analogs through Laboratory Experiments and Electron Microscopy Analysis, PSJ, 5, 248
Bradley, J. P. 1994, Chemically Anomalous, Preaccretionally Irradiated Grains in Interplanetary Dust from Comets, Sci, 265, 925
Brunetto, R., Romano, F., Blanco, A., et al. 2006, Space Weathering of Silicates Simulated by Nanosecond Pulse UV Excimer Laser, Icar, 180, 546
Brunetto, R., & Strazzulla, G. 2005, Elastic Collisions in Ion Irradiation Experiments: A Mechanism for Space Weathering of Silicates, Icar, 179, 265
Cantando, E. D., Dukes, C. A., Loeffler, M. J., & Baragiola, R. A. 2008, Aqueous Depletion of Mg from Olivine Surfaces Enhanced by Ion Irradiation, JGRE, 113, E9
Chapman, C. R. 2004, Space Weathering of Asteroid Surfaces, AREPS, 32, 539
Chardon, E. S., Livens, F. R., & Vaughan, D. J. 2006, Reactions of Feldspar Surfaces with Aqueous Solutions, ESRv, 78, 1
Chaves, L. C., Thompson, M. S., Loeffler, M. J., et al. 2023, Evaluating the Effects of Space Weathering on Magnetite on Airless Planetary Bodies, Icar, 402, 115634
Daval, D., Sissmann, O., Menguy, N., et al. 2011, Influence of Amorphous Silica Layer Formation on the Dissolution Rate of Olivine at 90°C and Elevated pCO_2, ChGeo, 284, 193
Davoisne, C., Leroux, H., Frère, M., et al. 2008, Chemical and Morphological Evolution of a Silicate Surface under Low-energy Ion Irradiation, A&A, 482, 541
DeMeo, F., Alexander, C., Walsh, K., et al. 2015, The Compositional Structure of the Asteroid Belt, Asteroids IV (Univ. Arizona Press), 13
Demyk, K., Carrez, Ph., Leroux, H., et al. 2001, Structural and Chemical Alteration of Crystalline Olivine under Low Energy He+ Irradiation, A&A, 368, L38
Dukes, C. A., Baragiola, R. A., & McFadden, L. A. 1999, Surface Modification of Olivine by H+ and He+ Bombardment, JGR, 104, 1865
Fairley, N., Fernandez, V., Richard-Plouet, M., et al. 2021, Systematic and Collaborative Approach to Problem Solving Using X-ray Photoelectron Spectroscopy, Appl. Surf. Sci. Adv., 5, 100112
Gosling, J. T. 2014, The Solar Wind, Encyclopedia of the Solar System (Elsevier), 261
Hapke, B. 1970, Inferences from the Optical Properties of the Moon Concerning the Nature and Evolution of the Lunar Surface, RaSc, 5, 293
Hapke, B. 2001, Space Weathering from Mercury to the Asteroid Belt, JGR, 106, 10039
Jäger, C., Fabian, D., Schrempel, F., et al. 2003, Structural Processing of Enstatite by Ion Bombardment, A&A, 401, 57
Kanamaru, M., Sasaki, S., Morota, T., et al. 2021, YORP Effect on Asteroid 162173 Ryugu: Implications for the Dynamical History, JGRE, 126, e2021JE006863
Keller, L. P., & McKay, D. S. 1993, Discovery of Vapor Deposits in the Lunar Regolith, Sci, 261, 1305
Keller, L. P., & McKay, D. S. 1997, The Nature and Origin of Rims on Lunar Soil Grains, GeCoA, 61, 2331
Kleiv, R. A., & Thornhill, M. 2006, Mechanical Activation of Olivine, MiEng, 19, 340
Kosuge, K., Shimada, K., & Tsunashima, A. 1995, Micropore Formation by Acid Treatment of Antigorite, ChMat, 7, 2241
Lafay, R., Montes-Hernandez, G., Janots, E., et al. 2014, Simultaneous Precipitation of Magnesite and Lizardite from Hydrothermal Alteration of Olivine under High-carbonate Alkalinity, ChGeo, 368, 63
Lauretta, D. S., Bartels, A. E,, Barucci, M. A., et al. 2015, The OSIRIS-REx Target Asteroid (101955) Bennu: Constraints on Its Physical, Geological, and Dynamical Nature from Astronomical Observations, M&PS, 50, 834
Lauretta, D. S., Connolly, H. C., Jr., Aebersold, J. E., et al. 2024, Asteroid (101955) Bennu in the Laboratory: Properties of the Sample Collected by OSIRIS-REx, M&PS, 59, 2453
Loeffler, M. J., Baragiola, R. A., & Murayama, M. 2008, Laboratory Simulations of Redeposition of Impact Ejecta on Mineral Surfaces, Icar, 196, 285
Loeffler, M. J., Dukes, C. A., & Baragiola, R. A. 2009, Irradiation of Olivine by 4 keV He+: Simulation of Space Weathering by the Solar Wind, JGRE, 114, E3
Loeffler, M. J., Dukes, C. A., Christoffersen, R., & Baragiola, R. A. 2016, Space Weathering of Silicates Simulated by Successive Laser Irradiation: In Situ Reflectance Measurements of Fo_{90}, Fo_{99+}, and SiO_2, M&PS, 51, 261
Matsuoka, M., Nakamura, T., Hiroi, T., Okumura, S., & Sasaki, S. 2020, Space Weathering Simulation with Low-energy Laser Irradiation of Murchison CM Chondrite for Reproducing Micrometeoroid Bombardments on C-type Asteroids, ApJL, 890, L23
Moulder, J. F., Stickle, W. F., Sobol, P. E., & Bomben, K. D. 1992, Handbook of X-ray Photoelectron Spectroscopy (Perkin-Elmer Corporation), 221
Nakauchi, Y., Abe, M., Ohtake, M., et al. 2021, The Formation of H_2O and Si-OH by H_2^+ Irradiation in Major Minerals of Carbonaceous Chondrites, Icar, 355, 114140
Noguchi, T., Matsumoto, T., Miyake, A., et al. 2024, Mineralogy and Petrology of Fine-grained Samples Recovered from the Asteroid (162173) Ryugu, M&PS, 59, 1877
Pieters, C. M., & Noble, S. K. 2016, Space Weathering on Airless Bodies, JGRE, 121, 1865
Pokrovsky, O. S., & Schott, J. 2000a, Forsterite Surface Composition in Aqueous Solutions: A Combined Potentiometric, Electrokinetic, and Spectroscopic Approach, GeCoA, 64, 3299
Pokrovsky, O. S., & Schott, J. 2000b, Kinetics and Mechanism of Forsterite Dissolution at 25 C and pH from 1 to 12, GeCoA, 64, 3313
Powell, C. J., Erickson, N. E., & Madey, T. E. 1979, Results of a Joint Auger/ESCA Round Robin Sponsored by Astm Commitee E-42 on Surface Analysis: Part I. Esca Results, JESRP, 17, 361
Prince, B. S., Magnuson, M. P., Chaves, L. C., Thompson, M. S., & Loeffler, M. J. 2020, Space Weathering of FeS Induced via Pulsed Laser Irradiation, JGRE, 125, e2019JE006242
Ragan, D. M. 1963, Emplacement of the Twin Sisters Dunite, Washington, AmJS, 261, 549
Rivkin, A. S., Howell, E. S., & Emery, J. P. 2019, Infrared Spectroscopy of Large, Low-albedo Asteroids: Are Ceres and Themis Archetypes or Outliers?, JGRE, 124, 1393
Sasaki, S., Kurahashi, E., Yamanaka, C., & Nakamura, K. 2003, Laboratory Simulation of Space Weathering: Changes of Optical Properties and TEM/ESR Confirmation of Nanophase Metallic Iron, AdSpR, 31, 2537
Schrenk, M. O., Brazelton, W. J., & Lang, S. Q. 2013, Serpentinization, Carbon, and Deep Life, RvMG, 75, 575
Seah, M. P., & Dench, W. A. 1979, Quantitative Electron Spectroscopy of Surfaces: A Standard Data Base for Electron Inelastic Mean Free Paths in Solids, SurIA, 1, 2
Shirley, D. A. 1972, High-resolution X-ray Photoemission Spectrum of the Valence Bands of Gold, PhRvB, 5, 4709
Takir, D., Emery, J. P., & McSween, H. Y. 2015, Toward an Understanding of Phyllosilicate Mineralogy in the Outer Main Asteroid Belt, Icar, 257, 185
Teir, S., Revitzer, H., Eloneva, S., Fogelholm, C.-J., & Zevenhoven, R. 2007, Dissolution of Natural Serpentinite in Mineral and Organic Acids, IJMP, 83, 36
Thompson, M. S., Morris, R. V., Clemett, S. J., et al. 2020, The Effect of Progressive Space Weathering on the Organic and Inorganic Components of a Carbonaceous Chondrite, Icar, 346, 113775
Wentworth, S. J., Keller, L. P., McKay, D. S., & Morris, R. V. 1999, Space Weathering on the Moon: Patina on Apollo 17 Samples 75075 and 76015, M&PS, 34, 593
Wogelius, R. A., & Walther, J. V. 1991, Olivine Dissolution at 25°C: Effects of pH, CO_2, and Organic Acids, GeCoA, 55, 943
Yada, T., Abe, M., Okada, T., et al. 2022, Preliminary Analysis of the Hayabusa2 Samples Returned from C-type Asteroid Ryugu, NatAs, 6, 214
Yoo, K., Kim, B.-S., Kim, M.-S., Lee, J.-c., & Jeong, J. 2009, Dissolution of Magnesium from Serpentine Mineral in Sulfuric Acid Solution, MatTr , 50, 1225
Ziegler, J. F., Ziegler, M. D., & Biersack, J. P. 2010, SRIM—The Stopping and Range of Ions in Matter (2010), NIMPB, 268, 1818